Behaviour of 3,4-Dihydroxy-9,10-Anthraquinone-2-Sulfonic Acid in Alkaline Medium: Towards a Long-Cycling Aqueous Organic Redox Flow Battery

Solene Guiheneuf, Aurore Le, Thibault Godet-Bar, Lea Chancelier, Jean-Marie Fontmorin, Didier Floner, Florence Geneste

Behaviour of 3,4-dihydroxy-9,10-anthraquinone-2-sulfonic acid in alkaline medium: towards a long-cycling aqueous organic redox flow battery

Solène Guiheneuf,[a,c] Aurore Lê,[a,b,c] Thibault Godet-Bar,[b] Léa Chancelier,[b] Jean-Marie Fontmorin,[a] Didier Floner[a] and Florence Geneste [a*]

[a] Dr Solène Guiheneuf, Dr Aurore Lê, Dr Jean-Marie Fontmorin, Dr Didier Floner, Dr Florence Geneste, Univ Rennes, CNRS, ISCR-UMR 6226, F-35000 Rennes, France

[b] Dr Thibault Godet-Bar, Dr Léa Chancelier, Kemiwatt, 11 allée de Beaulieu - CS 50837, F-35708 Rennes cedex 7, France.

[c] Equally contributing

ABSTRACT

The performance of a redox compound in redox flow batteries highly depends on the electrolytic medium and operating conditions. It is exemplified in this work with the commercially available and relatively low-cost dye 3,4-dihydroxy-9,10-anthraquinone-2-sulfonic acid (ARS), which was used as negolyte in basic medium. At high pH, ARS behavior revealed interesting features for RFB application such as a low half-wave potential of -0.99 V *vs* Ag/AgCl negatively shifted by phenolate groups and an improved solubility compared with acidic medium depending on the nature of cations. For the highly soluble ARS potassium salt (**ARSK**), a maximum power density of 117 mW cm^{-2} and a demonstrated energy density of 20

* florence.geneste@univ-rennes1.fr

Wh L^{-1} were obtained with $K_4[Fe(CN)_6]$ as posolyte. The capacity slightly decreased during cycling, reaching 90% after 325 cycles. A long cycling of ARS sodium salt (**ARSNa**) over 11 operating months was demonstrated in this work. A slow chemical degradation was highlighted giving rise to the formation of 3-hydroxy-9,10-anthraquinone-2-sulfonic acid (**HAQS**) as the main degradation product due to hydrodeoxygenation reaction. Interestingly, this compound exhibited high performance in RFB and a good stability with a loss of capacity of 0.29% per day.

1. Introduction

Aqueous organic redox flow batteries (AORFBs) have emerged as a cost-effective solution with expected low environmental impact to optimize renewable energies production due to their high storage capacity and a flexible energy to power ratio.[1] To make a water-based redox flow battery competitive with respect to traditional batteries for the storage of intermittent energy, it must comply with a number of requirements in terms of performances: energy density > 20 Wh L^{-1} corresponding to vanadium technology,[2] voltage > 1 V, durability (capacity loss < 0.003%/day for 20 years i.e. 0.003%/cycle for 1 full cycle of 10h per day) and cost (price of electrolyte < 110 € kW h^{-1} [3]). To achieve this goal, a large variety of electrolyte solutions has been studied.[4] Quinones and particularly anthraquinones have been considered as interesting negolytes in AORFBs owing to their reversible two-electron redox system. For example, the high solubility of 9,10-anthraquinone-2,7-disulfonate (AQDS) (up to 1 M at pH 0) would allow to reach a theoretical energy density of 50 Wh L^{-1} when combined with bromine.[1a] However, such high energy density has not been achieved yet in operating conditions. The low-cost

system involving 9,10-anthraquinone-2,7-disulfonate (AQDS) *versus* bromine in acidic medium exhibited interesting properties but bromine stabilization and membrane fouling limit the stability of the battery.[5] 2,6-dihydroxyanthraquinone (2,6-DHAQ) *versus* ferrocyanide in alkaline medium allowed reaching a theoretical energy density of 6.8 Wh L^{-1}, while under cycling operations, stabilities with 0.1% loss in capacity per cycle were exhibited.[2] Recent advances with 2,6-dihydroxyanthraquinone modified by alkyl-carboxylic acid groups led to a theoretical energy density of 12-17 Wh L^{-1}, although this value was not reached in operating conditions.[6] A capacity fade rate of 0.05%/day (0.001%/cycle) was obtained over a 5-day testing period. Alizarin-3-methyliminodiacetic acid *versus* ferrocyanide in alkaline medium has also shown an acceptable cycling performance for 350 cycles with a capacity loss of 0.02% per cycle at a current density of 0.1 A cm^{-2}.[7]

While most of the articles focus on new synthesized redox anthraquinones with improved solubility and chemical stability, less attention has been paid to the role of the electrolytic medium and operating conditions on their performances in AORFB.[1j, 4c, 8] However, each redox compound should be tested in optimized conditions in terms of pH, ionic environment, battery cycling parameters, etc., before concluding on its performances in AORFB.

It is exemplified in this work with the demonstrated performances of an AORFB over more than 11 operating months (5000 cycles) with the commercially available and relatively low-cost dye 3,4-dihydroxy-9,10-anthraquinone-2-sulfonic acid (ARS) *versus* ferrocyanide in alkaline medium. Whereas a maximum power density of 10.6 mW cm^{-2} and an energy density around 1 Wh L^{-1} have been previously reported in acidic medium with the ARS sodium salt (**ARSNa**) (Scheme 1),[9] much higher values, respectively 117 mW cm^{-2} and 7 Wh L^{-1}, were reached in alkaline medium. This is due to the presence of phenolate groups on anthraquinone that shifts negatively its redox potential to -0.99 V *vs* Ag/AgCl and improves its solubility. A demonstrated energy density up to 20 Wh L^{-1} could be even reached using the highly soluble

potassium salt of ARS (**ARSK**). The achievement of an 11 months-long cycling test was due to a slow chemical transformation of **ARSNa** during cycling into another redox active anthraquinone, 3-hydroxy-9,10-anthraquinone-2-sulfonic acid (**HAQS**). It corresponded to a degradation pathway of hydroxyanthraquinone that is reported for the first time in this work. The performances of this new redox anthraquinone derivative in RFB were also assessed.

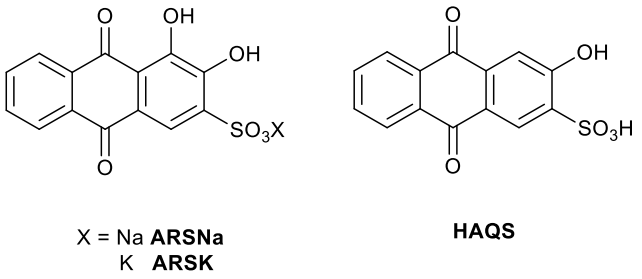

Scheme 1. Chemical structure of **ARSNa**, **ARSK** and **HAQS**

2. Results and discussion

*2.1. Physico-chemical properties of **ARSNa** in basic medium*

The pKas of all acidic functions of **ARSNa** were determined by titration to know the degree of deprotonation of the molecule according to the pH (Figures S1-3). The deprotonation of the sulfonic acid group occurred at pKa_1 = 2.2 and the first hydroxide group was deprotonated at pKa_2 = 6.3. The last pKa, corresponding to the deprotonation of the second hydroxide group was evaluated by UV measurements and found at 10.4 ± 0.9. Therefore, for a solution with a pH higher than 12 (i.e. pKa_3 + 2), 99% of the molecules in solution were completely deprotonated, which promotes the solubility of **ARSNa** in aqueous medium.

Cyclic voltammetry analysis of **ARSNa** in 2 mol L^{-1} potassium hydroxide is shown in Figure 1.

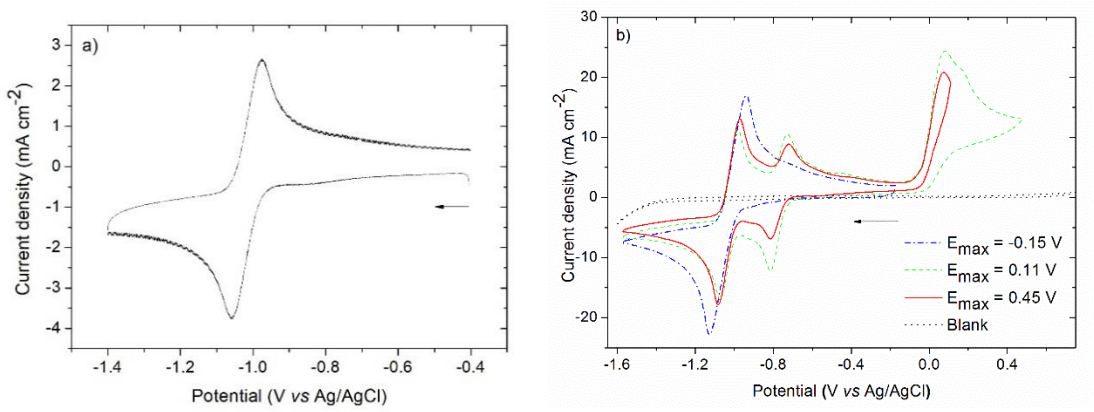

Figure 1. Cyclic voltammograms at a 0.071 cm^2 glassy carbon electrode of a a) 10^{-2} mol L^{-1} and b) 10^{-1} mol L^{-1} solution of **ARSNa** in a 2 mol L^{-1} KOH solution, 100 mV s^{-1}.

ARSNa presented a quasi-reversible system at a half-wave potential of -0.99 V *vs* Ag/AgCl, which is negatively shifted by 0.34 V and 0.64 V compared with ARS in pH 7 and 0, respectively.[10] This result underlines the interest to use ARS in alkaline medium to increase the cell voltage. When the potential was set at 0.11 V *vs* Ag/AgCl (Figure 1b), a new reversible system appeared at -0.77 V *vs* Ag/AgCl, the intensity of which increased with cycling. The apparition of the new redox couple was thus directly linked to the oxidation occurring at 0.05 V. The oxidation of ARS has been previously observed and attributed to the oxidation of its hydroxide groups into ketones resulting in a four ketone groups molecule that decomposes into other side-products.[10b, 11] Therefore, the decomposition of ARS at positive potentials will be detrimental to the battery stability if crossover occurs. However, crossover of negatively charged anthraquinone is usually negligible as demonstrated with AQDS [5] and 2,6-DHAQ.[2] The effect of pH on ARS half-wave potential was studied between pH 12 and 14 (Figure S4). The potential decreased by 36 mV per pH units, which corresponds to a two-electron/one-proton process (Figure S4b). One of the hydroxyl groups of the hydroquinone form of ARS remains protonated in this range of pH. The diffusion coefficient of **ARSNa** at room temperature was determined from the Levich equation to be 6.2×10^{-7} cm^2 s^{-1} (Figure S5a). This

value is close to those previously reported in acidic (2.14 and 1.58 × 10^{-6} cm^2 s^{-1}) [9, 11b] and neutral media (2.88 × 10^{-6} cm^2 s^{-1}).[11b] The electron transfer rate constant k_s was estimated as 1.2 × 10^{-3} cm s^{-1} from the Tafel plot (Figure S5b,c).[12] This value is consistent with the rate constant determined previously in acidic medium (3.6 × 10^{-3} cm s^{-1}) [9] and is similar to other quasi-reversible anthraquinones.[1l, 4c, 7]

The influence of the cations on the solubility of the oxidized form of ARS was then studied. The solubilities in 2 mol L^{-1} KOH of commercially available ARS (**ARSNa**, purity 81%) and two ARS synthesized by oleum sulfonation of 2-hydroxyanthraquinone (**ARSNa***, sodium salt, purity 93% and **ARSK**, potassium salt, purity 87%) were compared by the shake-flask method. The commercial and synthesized sodium salts of ARS displayed a solubility of 0.28 mol L^{-1} and 0.33 mol L^{-1}, respectively (Table 1), which is three times higher than the highest solubility reported for alizarin (0.1 mol L^{-1}) [13] but significantly lower than 2,6-DHAQ (> 0.6 mol L^{-1}).[2] The presence of hydrophilic groups such as sulfonate and phenolate on the anthraquinone backbone improves its solubility.[10a] However, when the hydroxyl group is in position 1, the solubility is affected, as shown by the higher solubility of 2,6-DHAQ compared with ARS. The difference in solubility between commercial and synthesized ARS sodium salts underlines the importance of the inorganic salts in the solution. This is further highlighted by the higher solubility of **ARSK** (0.51 mol L^{-1}) compared with **ARSNa**, owing to the high effect of the nature of counterions on ARS solubility. This solubility increase could be due to the higher radius of potassium that would decrease the bonding dissociation energy between anthraquinone and its counterion and would enhance the solvation of ARS anions in water.

2.2. Redox flow battery with ARS

Commercially available 0.2 mol L^{-1} **ARSNa** in 1.2 mol L^{-1} KOH was first tested in a redox flow battery with 0.5 mol L^{-1} $K_4[Fe(CN)_6]$ in 0.2 mol L^{-1} NaOH used as posolyte. The solubility of the reduced form of commercial **ARSNa** in the same electrolyte estimated in a glove box was

above 0.47 mol L^{-1}, suggesting that no solubility issue should be observed along charging sequences. Since Na^+ migration in the ion exchange membrane can affect the solubility of ARS, it is better to use the same initial Na^+ composition in the negolyte and posolyte, as it was done in this work. To check if the initial composition in Na^+ and K^+ ions of the positive and negative electrolytes is maintained during battery operation, Na^+ and K^+ ratios were quantified by ion chromatography at the end of charge and discharge (Figure 2a).

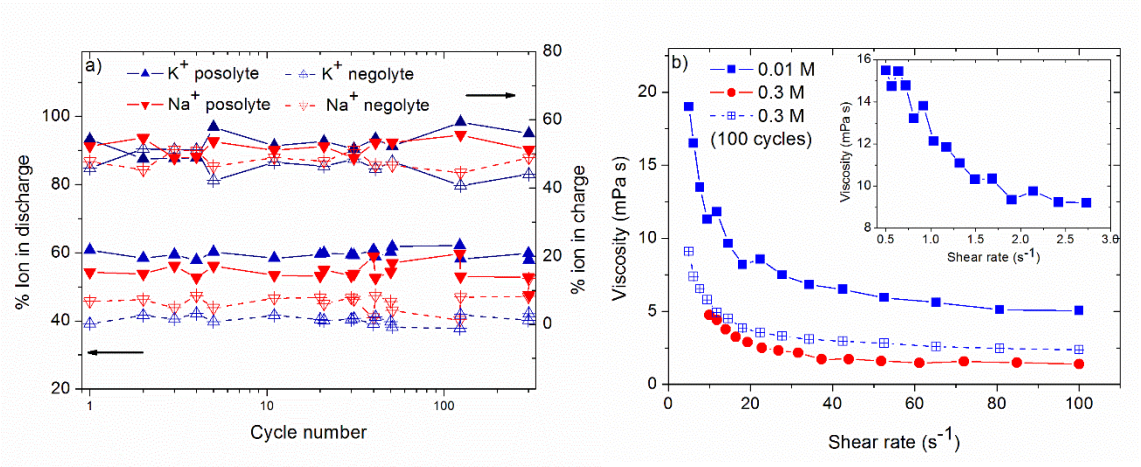

Figure 2. a) Relative Na^+ and K^+ analysis by ion chromatography for 0.5 mol L^{-1} $K_4[Fe(CN)_6]$ in 0.2 mol L^{-1} NaOH posolyte and 0.2 mol L^{-1} **ARSNa** in 1.2 mol L^{-1} KOH negolyte (40 mA cm^{-2}; cut-off voltage 1.5 V) in charge (top) and discharge (bottom) b) Shear rate dependence of the viscosity of **ARSNa** at 20°C at different concentrations and after 100 cycles in RFB. Inset 0.2 mol L^{-1} **ARSNa**.

The initial concentration of ions was stable during cycling with just the expected transfer due to electro-osmosis and/or osmosis during charge and discharge, preserving the solubility of ARS.

For a better understanding of the rheological behavior of the ARS solution, its viscosity was measured at different concentrations and shear rates (Figure 2b). Even at low ARS concentration for RFB application (0.01 mol L^{-1}), ARS solutions exhibited a non-Newtonian

rheofluidizing type profile since the viscosity decreased with the shear rate. Therefore, a good stirring of the solution will decrease its viscosity. The viscosity of a 0.2 mol L^{-1} **ARSNa** solution was also studied in the range 0.5-3.0 s^{-1} corresponding to low flow rates that are usually used in RFB stack to limit the pumping cost (Inset of Figure 2b). At 2.5 s^{-1}, a quite high viscosity around 9 mPa s was obtained, showing the importance of a good stirring of the electrolyte. Thus, for this first study, a high flow rate of 150 mL min^{-1} was used in RFB tests to limit problems linked to the thixotropic behavior of ARS.[10a] Interestingly, the viscosity of the solution significantly decreased after 100 cycles. This is a benefit for RFB owing to its impact on the mass transfer rates and on the pressure losses in the process (requires lower pumping power).[14]

A charge-discharge cycling with a charging protocol of constant current density at 40 mA cm^{-2} is presented in Figure 3 and its performances are summarized in Table 1.

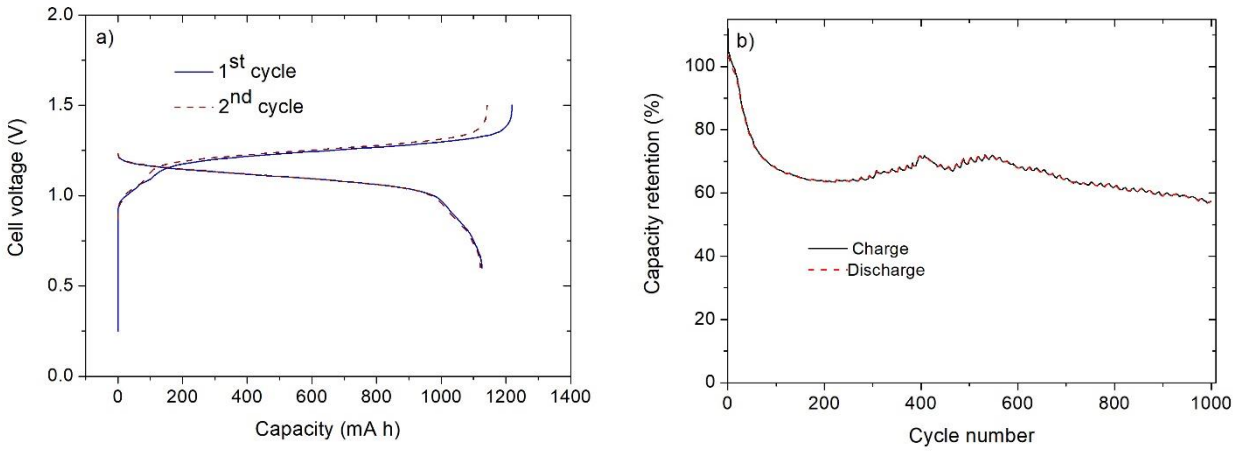

Figure 3. a) Charge-discharge curves of the two first cycles and b) evolution of the capacity with the cycle number for 0.5 mol L^{-1} $K_4[Fe(CN)_6]$ in 0.2 mol L^{-1} NaOH posolyte (100 mL) and 0.2 mol L^{-1} commercial ARS in 1.2 mol L^{-1} KOH negolyte (100 mL) (40 mA cm^{-2}; cut-off voltage 1.5 V)

A first plateau was observed around 1.05 V in charge and in discharge and its size increased during cycling (Figure 3a and S6). Furthermore, the capacity rapidly decreased during the 100 first cycles and stabilized at around 65% of the theoretical value. To check if this decrease in capacity was due to impurities present in commercial **ARSNa**, the synthesized sodium salt of ARS **ARSNa*** (93%) was tested in a redox flow battery in the same conditions (Figure S7). Although less pronounced, two plateaus were also observed in charge and discharge and the capacity rapidly decreased to reach around 70% of the theoretical value. The initial capacity loss can be attributed to several factors. First, the concentration of **ARSNa** (0.2 mol L^{-1}) is close to its solubility limit (0.28 mol L^{-1}), that could lead to the formation of small solid particles during cycling owing to cation exchange through the membrane and water transfer. Second, real-time monitoring of the battery state of charge (SOC) by linear sweep voltammetry analysis on a rotating disk electrode showed a SOC shift that decreased with the number of cycles (Figure 4).

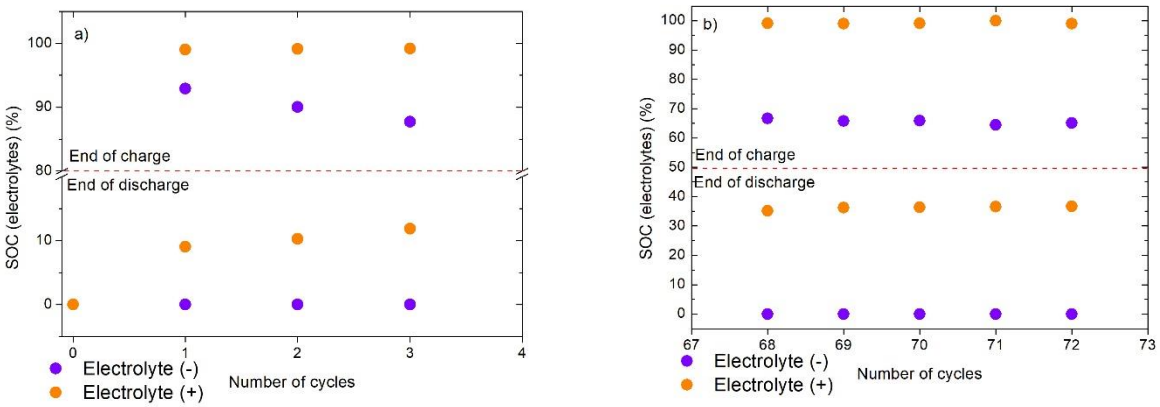

Figure 4. SOC of the electrolytes measured by LSV at a 0.071 cm^2 glassy carbon rotating disk electrode, rotation rate 1000 rpm and scan rate 20 mV s^{-1}. a) cycles 1 to 3, b) cycles 68 to 72.

At the end of the first charge, the posolyte SOC was close to 100%, whereas the negolyte showed a mixture of the oxidized and reduced forms of ARS. Since $K_4[Fe(CN)_6]$ in basic medium has previously shown high stability during cycling,[15] this could be explained by the occurrence of a side-reaction in the negolyte tank. Hydrogen evolution was a probable assumption considering the relative heterogeneous distribution of the potential inside a 3D porous electrode. The presence of two plateaus on the charge and discharge curves also suggested a degradation of ARS to another reversible electroactive compound.

To take advantage of its higher solubility and increase the capacity of the battery, a solution of 0.44 mol L^{-1} potassium salt of ARS **ARSK** in 1.7 mol L^{-1} KOH (50 mL) was implemented in a redox flow battery with 0.5 mol L^{-1} $K_4[Fe(CN)_6]$ in 0.2 mol L^{-1} NaOH (100 mL). A volume of 100 mL was used since potassium ferrocyanide is not soluble in the electrolyte at 0.88 mol L^{-1}. The performances of the battery are given in Figure 5 and summarized in Table 1.

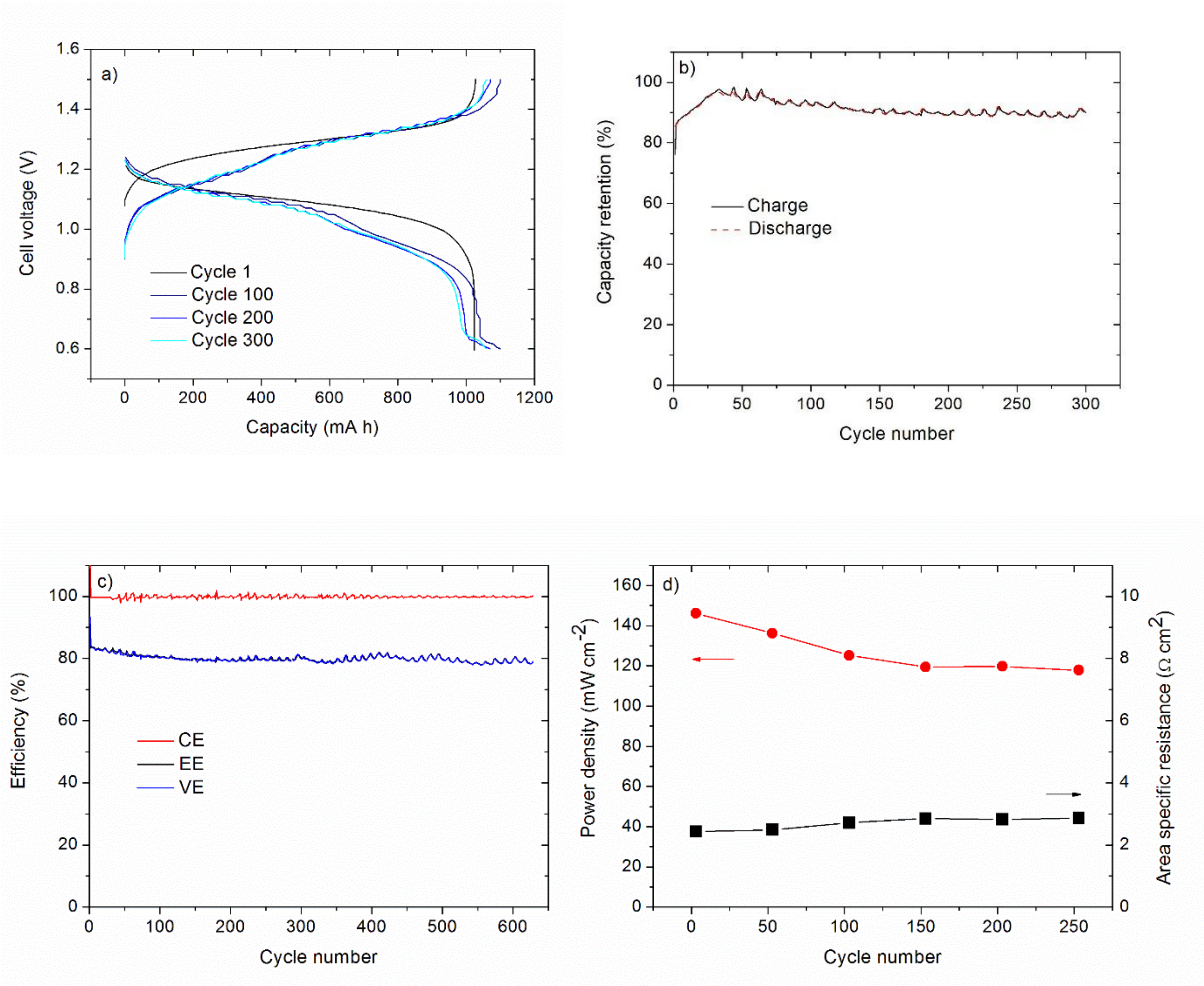

Figure 5. a) Charge-discharge curves and b) Evolution of the capacity with time according to the cycle numbers for 0.5 mol L^{-1} $K_4[Fe(CN)_6]$ in 0.2 mol L^{-1} NaOH posolyte (100 mL) and 0.44 mol L^{-1} ARS potassium salt **ARSK** in 1.7 mol L^{-1} KOH negolyte (50 mL) (40 mA cm^{-2}; cut-off voltage 1.5 V) c) Coulombic efficiency (CE), voltage efficiency (VE) and round-trip energy efficiency (EE) d) Maximum power density obtained by polarization curves performed at a 50% state of charge (SOC) and cell resistance *vs* number of cycles.

For this RFB with double the ARS concentration, a stable coulombic efficiency (CE) close to 100% and voltage (VE) and energy (EE) efficiencies of 80% were obtained for a current density of 40 mA cm^{-2}. These results were similar to the commercial and synthesized ARS sodium salts (Figure S8), although VE and EE values were slightly higher (around 83%). The round-trip

energy efficiency was also consistent with literature for anthraquinones used in aqueous organic redox flow batteries.[4c, 5-7] The maximum power density varied between 117 and 146 mW cm^{-2} during cycling showing similar values to ARS sodium salt **ARSNa** (115-200 mW cm^{-2}, Figure S9). It is consistent with the similarity of area specific resistances that were in the range of 2-2.9 Ω cm^2 for both compounds.

The energy densities of the RFB with potassium and sodium salts of ARS are given in Figure 6.

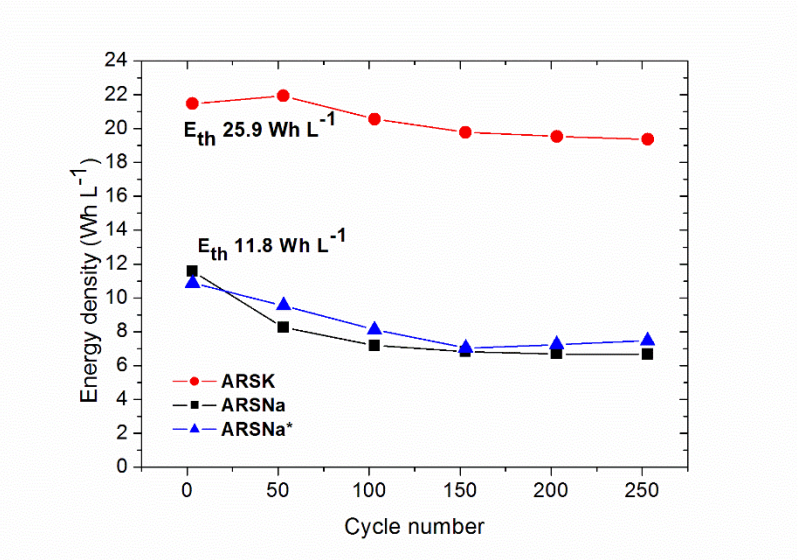

Figure 6. Energy density *vs* cycle number for RFB with 0.5 mol L^{-1} $K_4[Fe(CN)_6]$ in 0.2 mol L^{-1} NaOH posolyte (100 mL) and 0.44 mol L^{-1} ARS potassium salt **ARSK** in 1.7 mol L^{-1} KOH negolyte (50 mL) and 0.5 mol L^{-1} $K_4[Fe(CN)_6]$ in 0.2 mol L^{-1} NaOH posolyte and 0.2 mol L^{-1} commercial **ARSNa** and synthesized **ARSNa*** in 1.2 mol L^{-1} KOH negolyte. Eth: theoritical values of energy density.

The energy density of RFB with the ARS potassium salt **ARSK** was significantly higher than with the commercial and synthetic sodium salts of ARS, owing to its higher solubility in basic aqueous medium. After stabilization, it reached an experimental value of 20 Wh L^{-1} against 7

Wh L^{-1} for **ARSNa**. It is similar to the value of energy density (20 Wh L^{-1}) that is usually required for RFB. Since the energy density of a battery is the amount of energy stored in proportion to its total volume, it is interesting to consider both negolyte and posolyte volumes for its estimation. Indeed, it is more representative of industrial applications. It corresponded to a value of 6.7 Wh L^{-1} against 3.5 Wh L^{-1} for **ARSNa**, since a higher volume (100 mL) was considered for the posolyte compartment. Thus, the posolyte composition would have to be improved to take full advantage of the higher solubility of the **ARSK**. Interestingly, the initial decrease of capacity was less drastic than with **ARSNa** and reached 90% after 325 cycles (Figure 5b). A possible explanation is that the higher solubility of **ARSK** would prevent the formation of small solid particles and that a higher concentration of ARS would favour its reduction and limit the competition with hydrogen evolution.

2.3. Chemical degradation of ARS during cycling

Although RFB with ARS potassium salt **ARSK** exhibited very interesting performances in terms of coulombic and energy efficiencies, power density and energy density, the charge and discharge curves also exhibited two plateaus that increased during cycling (Figure 5a). Since the formation of new species was suspected, a long RFB cycling (5000 cycles) was carried out with 0.5 mol L^{-1} $K_4[Fe(CN)_6]$ in 0.2 mol L^{-1} NaOH posolyte and 0.2 mol L^{-1} commercial **ARSNa** in 1.2 mol L^{-1} KOH negolyte (Figure S10). After cycling, the negolyte solution was analyzed by cyclic voltammetry, mass spectroscopy and ^{1}H NMR. Cyclic voltammetry analysis (Figure S11a) revealed the presence of a new reversible system at -0.81 V *vs.* Ag/AgCl that increased with the number of cycles. It shows that ARS was degraded in a main by-product that still contained the electroactive anthraquinone backbone.

MS analyses also underlined the presence of a main by-product with the molecular formula $C_{14}H_8O_6S$ with another compound of higher molecular mass ($C_{28}H_{14}O_{10}S_2$) corresponding probably to a dimer. ^{1}H NMR performed in DMSO-d_6 showed that the molecule exhibited 6

CH signals, 4 coupling aromatic protons and 2 uncoupling aromatic protons, whereas the peaks corresponding to ARS were very small (Figure S11b).

From these data, 3-hydroxy-9,10-anthraquinone-2-sulfonic acid (**HAQS**) (Scheme 1) was proposed to be a by-product formed during ARS cycling.

To attest the molecular structure of this main by-product **HAQS**, it was synthesized from 2-hydroxyanthraquinone. It exhibited a reversible system in cyclic voltammetry at -0.81 V *vs.* Ag/AgCl, which is at the same position that the new reversible system formed during cycling (Figure S11a). It is interesting to note that the potential of the reversible system corresponding to this new by-product (-0.81 V *vs.* Ag/AgCl) is different from the by-product formed during cyclic voltammetry analysis (-0.77 V *vs.* Ag/AgCl, Figure 1). The comparison of **HAQS** with the bulk solution after RFB cycling was also performed in UV-vis analysis (Figure S11c). The spectrum of the synthesized **HAQS** perfectly matched that of the bulk solution after RFB operation, confirming that **HAQS** was the main product of ARS degradation. Compared with **ARSNa**, the n→π* absorption band between 500 and 630 nm due to $S_{n\rightarrow\pi^*}$ electronic transitions was blue-shifted with a peak at 475 nm due to the loss of an auxochrome hydroxyl group.[16] This is in agreement with cyclic voltammetry analyses (Figure S11a), showing that the potential of the new reversible system was anodically shifted owing to the loss of the donor hydroxyl group.

Degradation products of quinones in RFB have been previously linked to Michael addition/substitution by water or gem-diol formation and to disproportionation leading to the formation of anthrone.[3a, 17] However, the formation of **HAQS** cannot be attributed to these reactions. A possible explanation would be a hydrodeoxygenation reaction during water electrolysis [18] or a spontaneous degradation of the reduced form of ARS. The mechanism for the formation of the minor by-product ($C_{28}H_{14}O_{10}S_2$) could involve a dimerization reaction of radical intermediates, supported by the recent demonstration of radical formation during

anthraquinone reduction.[19] If the degradation is linked to the high voltage cut-off (1.5 V) used during the charge process, a less negative value could be used adding a constant voltage step.[15] However, it would lead to a longer charge time.

*2.4. Redox flow battery with **HAQS***

Although ARS degradation occurred during RFB operation, the high stability of the battery when 60% capacity was reached led us to evaluate the performances of synthesized **HAQS** in a RFB composed of 0.5 mol L^{-1} $K_4[Fe(CN)_6]$ in 0.2 mol L^{-1} NaOH as posolyte and 0.2 mol L^{-1} **HAQS** in 1.2 mol L^{-1} KOH / 0.2 mol L^{-1} NaOH as negolyte. A charge-discharge cycling with a charging protocol of constant current density at 40 mA cm^{-2} is presented in Figure 7.

10.1002/celc.202100284

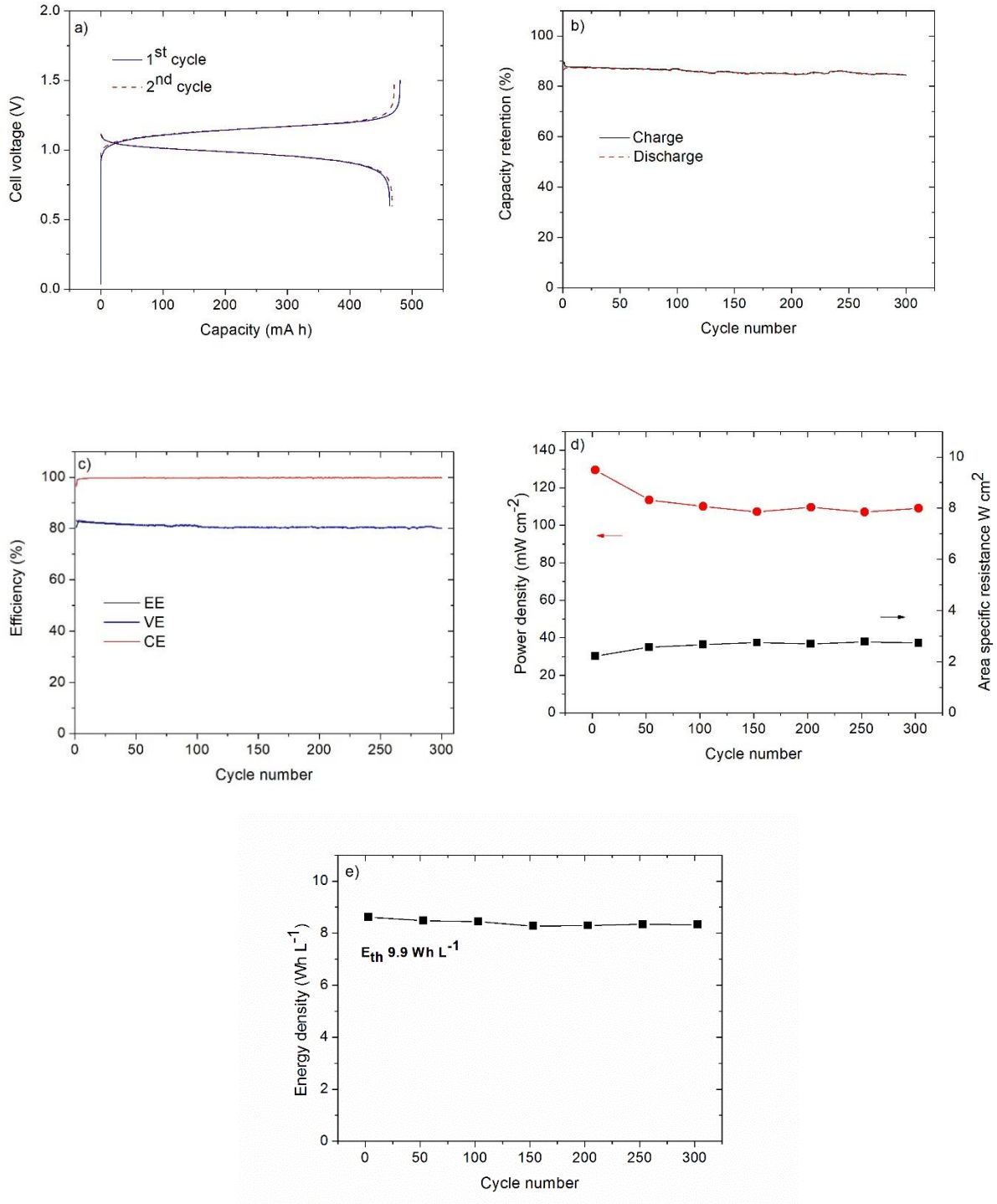

Figure 7. a) Charge-discharge curves of the two first cycles and b) evolution of the capacity with the cycle number for 0.5 mol L^{-1} $K_4[Fe(CN)_6]$ in 0.2 mol L^{-1} NaOH posolyte (100 mL) and 0.2 mol L^{-1} **HAQS** in 1.2 mol L^{-1} KOH / 0.2 mol L^{-1} NaOH negolyte (50 mL) (40 mA cm^{-2}; CV 1.5 V) c) Coulombic efficiency (CE), voltage efficiency (VE) and round-trip energy efficiency (EE) d) Maximum power density obtained by polarization curves performed at a 50%

state of charge (SOC) and cell resistance *vs* number of cycles e) Energy density *vs* cycle number. Eth: theoretical value of energy density.

The charge-discharge curves (Figure 7a) did not display several plateaus as for ARS, confirming the link between the presence of plateaus and the formation of new species, especially **3**. A loss of capacity of 0.012% per cycle corresponding to 0.29% per day was calculated between cycles 10 and 300, underlining the high stability of **HAQS** in RFB. It is important to note that this stability estimation was obtained in classical operating conditions that do not allow the elimination of all traces of dioxygen.

As for ARS potassium and sodium salts **ARSNa** and **ARSK**, the coulombic efficiency was close to 100% and the voltage and energy efficiencies were around 80% (Figure 7c), underlining that **HAQS** had also a very high round-trip energy efficiency. The area specific resistance increased during the first 50 cycles to reach a value of 2.7 Ω cm^2 (Figure 7d), which is similar to those obtained with **ARSNa** and **ARSK**. It directly affected the power density, decreasing from 129 mW cm^{-2} to 109 mW cm^{-2}. This value is slightly lower than for **ARSNa** (117 mW cm^{-2}) owing to the higher half-wave potential of **HAQS** (-0.81 V *vs.* Ag/AgCl) compared with **ARSNa** (-0.99 V *vs.* Ag/AgCl).

RFB with the anthraquinone derivative **HAQS** exhibited an energy density of 8,3 Wh L^{-1} (Figure 7e), which was slightly higher than for RFB with **ARSNa** performed with the same concentration of redox species after stabilization (7 Wh L^{-1}). The energy density is directly proportional to the average discharge voltage and to the average discharge capacity. Since a 180 mV decrease of the difference of potential was expected from cyclic voltammetry analysis, the higher energy density was due to the presence of other by-products during RFB operation with ARS, although **HAQS** was clearly the main one (around 75%).

Table 1. Characteristics of the redox flow batteries

Compound	$E_{1/2}$ (V *vs.* Ag/AgCl)	Solubility [a] (mol L^{-1})	Energy density [b,c] (Wh L^{-1})	Maximum power density (mW cm^{-2})	ASR W cm^{-2}	CE[b] %	EE[b] %	VE[b] %
Commercial **ARSNa** [d]	-0.99	0.28	7	145-182	1.9-2.4	~100	83	83
Synthesized **ARSNa*** [d]	-0.99	0.33	7	155-200	2-2.8	~100	83	83
Synthesized **ARSK** [d]	-0.99	0.51	20	117-147	2.4-2.9	~100	79	79
HAQS [e]	-0.81	-	8.3	109-129	2.2-2.7	~100	80	80
ARS[f]	-0.35	< 0.05	~1	10.6	-	-	-	-

[a] in 2 mol L^{-1} KOH [b] After stabilization [c] Considering the volume of anolyte [d] 0.5 mol L^{-1} $K_4[Fe(CN)_6]$ in 0.2 mol L^{-1} NaOH posolyte and 0.2 mol L^{-1} **ARSK** in 1.2 mol L^{-1} KOH negolyte [e] 0.5 mol L^{-1} $K_4[Fe(CN)_6]$ in 0.2 mol L^{-1} NaOH posolyte and 0.2 mol L^{-1} **HAQS** in 1.2 mol L^{-1} KOH / 0.2 mol L^{-1} NaOH negolyte [f] Ref. 9 and 10 in 1 mol L^{-1} H_2SO_4.

3. Conclusions

The emergence of new organic redox species showing high performances in RFB, makes them attractive as a storage solution for intermittent energies. However, the nature of the surrounding

electrolytic environment has also a lot of influence on the performance of RFB. This study on ARS as negolyte in basic medium for RFB is behind these findings. The main following parameters have been underlined:

- The ARS half-wave potential was negatively shifted, increasing the cell voltage.

- The solubility is improved and is positively influenced by the nature of cations, as shown by the highest solubility of **ARSK** (0.51 mol L^{-1}) compared with that of **ARSNa** (0.33 mol L^{-1}). Their effect is not limited to the oxidized state of the molecule and affects the solubility of its reduced state estimated at 0.47 mol L^{-1} for commercial **ARSNa**, meaning twice the value of its oxidized state.

- The nature of cations influences the solubility of the posolyte. To allow **ARSK** to be tested in RFB at a concentration of 0.44 mol L^{-1}, the volume of posolyte must be doubled since potassium ferrocyanide is not soluble in water at 0.88 mol L^{-1}. The equilibration of cations by electro-osmosis and osmosis during cycling, along with water transfer, is expected to increase the complexity of the system.

- The purity of redox species becomes an essential parameter too. For **ARSNa**, the improvement of the purity (93%) of the synthesized compound compared with the commercial one (81%) slightly increased its solubility from 0.28 to 0.33 mol L^{-1}.

- The conditions used for RFB cycling have also to be well adapted to the electrolytes. Thus, non-Newtonian fluids, such as ARS in basic medium require high stirring to decrease their viscosity. A compromise has to be found between the power consumption by pumps and the kinetics of charge transfer. The charge voltage cut-off is also an essential parameter to consider. It allows a good control of side-reactions such as water electrolysis, minimizing electrolyte imbalance.

To conclude, ARS sodium salt **ARSNa** exhibited good performances in terms of coulombic efficiency (100%) and voltage and round-trip energy efficiency (around 83%). A good power density (117 mW cm^{-2}) and a high demonstrated energy density (20 Wh L^{-1}) were also achieved with **ARSK**. A good stability with a capacity loss of only 0.012% per cycle corresponding to 0.29% per day was obtained with **HAQS**, while **ARSNa** could be cycling over 11 operating months.

Acknowledgments

A. Lê thanks ANRT and Kemiwatt for her Ph.D grant. The authors thank la Région Bretagne and BPI France (Concours Mondial de l'Innovation) for financial support.

References

[1] a) B. Huskinson, M. P. Marshak, C. Suh, S. Er, M. R. Gerhardt, C. J. Galvin, X. Chen, A. Aspuru-Guzik, R. G. Gordon, M. J. Aziz, *Nature* **2014**, *505*, 195-198; b) A. Hollas, X. Wei, V. Murugesan, Z. Nie, B. Li, D. Reed, J. Liu, V. Sprenkle, W. Wang, *Nat. Energy* **2018**, *3*, 508-514; c) K. Lin, R. Gomez-Bombarelli, E. S. Beh, L. Tong, Q. Chen, A. Valle, A. Aspuru-Guzik, M. J. Aziz, R. G. Gordon, *Nat. Energy* **2016**, *1*, 16102; d) A. Orita, M. G. Verde, M. Sakai, Y. S. Meng, *Nat. Commun.* **2016**, *7*, 13230; e) T. Janoschka, N. Martin, M. D. Hager, U. S. Schubert, *Angew. Chem., Int. Ed.* **2016**, *55*, 14427-14430; f) T. Janoschka, N. Martin, U. Martin, C. Friebe, S. Morgenstern, H. Hiller, M. D. Hager, U. S. Schubert, *Nature* **2015**, *527*, 78-81; g) E. S. Beh, D. De Porcellinis, R. L. Gracia, K. T. Xia, R. G. Gordon, M. J. Aziz, *ACS Energy Lett.* **2017**, *2*, 639-644; h) B. Yang, L. Hoober-Burkhardt, S. Krishnamoorthy, A. Murali, G. K. S. Prakash, S. R. Narayanan, *J. Electrochem. Soc.* **2016**, *163*, A1442-A1449; i) L. Hoober-Burkhardt, S. Krishnamoorthy, B. Yang, A. Murali, A. Nirmalchandar, G. K. S.

Prakash, S. R. Narayanan, *J. Electrochem. Soc.* **2017**, *164*, A600-A607; j) W. Lee, G. Park, Y. Kim, D. Chang, Y. Kwon, *Chem. Eng. J.* **2020**, *398*, 125610; k) J. D. Hofmann, F. L. Pfanschilling, N. Krawczyk, P. Geigle, L. Hong, S. Schmalisch, H. A. Wegner, D. Mollenhauer, J. Janek, D. Schroeder, *Chem. Mater.* **2018**, *30*, 762-774; l) W. Lee, A. Permatasari, B. W. Kwon, Y. Kwon, *Chem. Eng. J.* **2019**, *358*, 1438-1445; m) Z. Li, Y.-C. Lu, *Chem* **2018**, *4*, 2020-2021; n) J. D. Hofmann, S. Schmalisch, S. Schwan, L. Hong, H. A. Wegner, D. Mollenhauer, J. Janek, D. Schroeder, *Chem. Mater.* **2020**, *32*, 3427-3438; o) Z. Li, Y.-C. Lu, *Adv. Mater.* **2020**, *32*, 2002132; p) W. Lee, G. Park, Y. Kwon, *Chem. Eng. J.* **2020**, *386*, 123985; q) S. Schwan, D. Schroeder, H. A. Wegner, J. Janek, D. Mollenhauer, *ChemSusChem* **2020**, *13*, 5480-5488; r) H. Chen, G. Cong, Y.-C. Lu, *J. Energy Chem.* **2018**, *27*, 1304–1325.

[2] K. Lin, Q. Chen, M. R. Gerhardt, L. Tong, S. B. Kim, L. Eisenach, A. W. Valle, D. Hardee, R. G. Gordon, M. J. Aziz, M. P. Marshak, *Science* **2015**, *349*, 1529-1532.

[3] a) D. G. Kwabi, Y. Ji, M. J. Aziz, *Chem. Rev.* **2020**, *120 (14)*, 6467–6489; b) R. M. Darling, K. G. Gallagher, J. A. Kowalski, S. Ha, F. R. Brushett, *Energy Environ. Sci.* **2014**, *7*, 3459-3477.

[4] a) T. Hagemann, J. Winsberg, M. Grube, I. Nischang, T. Janoschka, N. Martin, M. D. Hager, U. S. Schubert, *J. Power Sources* **2018**, *378*, 546-554; b) B. Hu, C. DeBruler, Z. Rhodes, T. L. Liu, *J. Am. Chem. Soc.* **2017**, *139*, 1207-1214; c) B. Hu, J. Luo, M. Hu, B. Yuan, T. L. Liu, *Angew. Chem., Int. Ed.* **2019**, *58*, 16629-16636; d) Y. Huo, X. Xing, C. Zhang, X. Wang, Y. Li, *RSC Adv.* **2019**, *9*, 13128-13132; e) Y. Y. Lai, X. Li, K. Liu, W.-Y. Tung, C.-F. Cheng, Y. Zhu, *ACS Appl. Energy Mater.* **2020**, *3*, 2290-2295.

[5] Q. Chen, L. Eisenach, M. J. Aziz, *J. Electrochem. Soc.* **2016**, *163*, A5057-A5063.

[6] D. G. Kwabi, K. Lin, Y. Ji, E. F. Kerr, M.-A. Goulet, D. De Porcellinis, D. P. Tabor, D. A. Pollack, A. Aspuru-Guzik, R. G. Gordon, M. J. Aziz, *Joule* **2018**, *2*, 1894-1906.

[7] Y. Liu, S. Lu, S. Chen, H. Wang, J. Zhang, Y. Xiang, *ACS Appl. Energy Mater.* **2019**, *2*, 2469-2474.

[8] A. Permatasari, W. Lee, Y. Kwon, *Chem. Eng. J.* **2020**, *383*, 123085.

[9] S. Zhang, X. Li, D. Chu, *Electrochim. Acta* **2016**, *190*, 737-743.

[10] a) K. Wedege, E. Drazevic, D. Konya, A. Bentien, *Sci. Rep.* **2016**, *6*, 39101; b) S. Schumacher, T. Nagel, F. W. Scheller, N. Gajovic-Eichelmann, *Electrochim. Acta* **2011**, *56*, 6607-6611.

[11] a) H. E. Zittel, T. M. Florence, *Anal. Chem.* **1967**, *39*, 320-326; b) B. Dadpou, D. Nematollahi, *J. Electrochem. Soc.* **2016**, *163*, H559-H565; c) L. B. Capeletti, J. H. Z. Dos Santos, E. Moncada, Z. N. Da Rocha, I. M. Pepe, *Powder Technol.* **2013**, *237*, 117-124; d) T. Ohsaka, N. Oyama, Y. Takahira, S. Nakamura, *J. Electroanal. Chem. Interfacial Electrochem.* **1988**, *247*, 339-343.

[12] A. J. Bard, L. R. Faulkner, *Electrochemical Methods: Fundamentals and Applications*, John Wiley & Sons, Inc, New York, **2001**.

[13] D. Floner, L. Paquin, S. Guiheneuf, F. Geneste, J.-P. Bazureau, (Universite de Rennes 1, Fr.; Centre National de la Recherche Scientifique). WO 2017212179, **2017**.

[14] a) J. D. Milshtein, R. M. Darling, J. Drake, M. L. Perry, F. R. Brushett, *J. Electrochem. Soc.* **2017**, *164*, A3883-A3895; b) J. L. Barton, J. D. Milshtein, J. J. Hinricher, F. R. Brushett, *J. Power Sources* **2018**, *399*, 133-143.

[15] A. Le, D. Floner, T. Roisnel, O. Cador, L. Chancelier, F. Geneste, *Electrochim. Acta* **2019**, *301*, 472-477.

[16] E. H. Anouar, C. P. Osman, J.-F. F. Weber, N. H. Ismail, *SpringerPlus* **2014**, *3*, 233/231-233/212.

[17] M.-A. Goulet, L. Tong, D. A. Pollack, D. P. Tabor, S. A. Odom, A. Aspuru-Guzik, E. E. Kwan, R. G. Gordon, M. J. Aziz, *J. Am. Chem. Soc.* **2019**, *141*, 8014-8019.

[18] a) S. Kim, E. E. Kwon, Y. T. Kim, S. Jung, H. J. Kim, G. W. Huber, J. Lee, *Green Chem.* **2019**, *21*, 3715-3743; b) Z. Si, X. Zhang, C. Wang, L. Ma, R. Dong, *Catalysts* **2017**, *7*, 169/161-169/122.

[19] E. W. Zhao, T. Liu, E. Jonsson, J. Lee, I. Temprano, R. B. Jethwa, A. Wang, H. Smith, J. Carretero-Gonzalez, Q. Song, C. P. Grey, *Nature* **2020**, *579*, 224-228.

Table of Contents

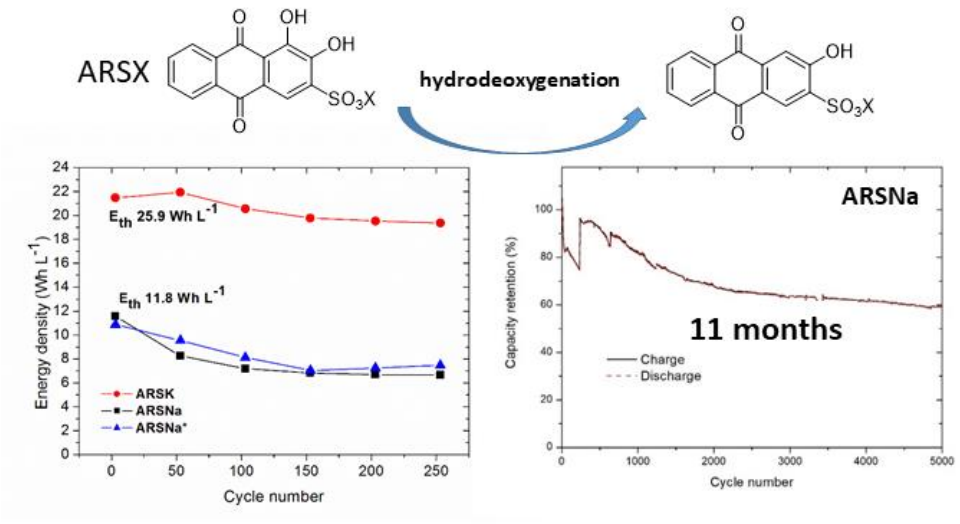

Basic electrolyte led to improved performance for ARS in AORFB, reaching a demonstrated energy density of 20 Wh L^{-1} for the highly soluble ARS potassium salt. A long cycling over 11

months was demonstrated, allowing the identification of a previously unknown degradation pathway of anthraquinone into new redox active species.

KEYWORDS: quinones, solubility, energy density, stability, redox chemistry